

Visualization of Spectroscopy for Remote Surface Operations

Mark W. Powell, Jeffrey S. Norris, Paul G. Backes
Jet Propulsion Laboratory, California Institute of Technology, Pasadena, California
Mark.Powell@jpl.nasa.gov

Abstract— This work discusses the role that in-situ spectroscopy plays in remote surface operations and how effective visualization of spectra can benefit planning. We begin by discussing how spectroscopy was used in the Mars Pathfinder mission and field trials with a prototype of the Mars Exploration Rover, paying close attention to shortcomings in visualization that hamper science planning. Next, we will introduce two methods for improving visualization of spectra that will be used during the Mars Exploration Rover 2003 mission: image cubes and data fusion. Image cubes view a collection of spectra as a hyperspectral image and allows spectra to be enhanced using image processing algorithms. Data fusion places spectral data in the context of a conventional image by overlaying an image cube slice onto an image of the terrain. We demonstrate these techniques with examples of image cubes and data fusion using data from FIDO rover field trials. We conclude with a discussion of future directions for these visualization methods.

TABLE OF CONTENTS

1. INTRODUCTION
2. ROVER-BASED SPECTROMETERS
3. IMAGE CUBES
4. DATA FUSION
5. RESULTS
6. SUMMARY

1. INTRODUCTION

It is arguable that in-situ spectroscopy is the most important scientific data that is returned from a planetary rover mission. Analyses of the spectroscopy data returned from the Pathfinder mission revealed a plethora of new information, such as the differing composition of rocks near the landing site from Martian meteorites found on Earth. Now these data are being compared to data from orbiters such as Mars Global Surveyor to locate the most scientifically lucrative sites for landing the next planetary rover missions, the two Mars Exploration Rovers (MER), to be launched in 2003. In this mission, two rovers will traverse the surface of Mars to search for signs of past or present life such as aqueously-deposited minerals.

Mission operations during Pathfinder allowed spectroscopy analysis to be done by visualizing the data as simple plots, as shown in Figure 1. These plots are a convenient visualization of a single observation, and were appropriate for the 28 total spectra that were returned from the mission [1]. In future rover missions, mast-based pointing spectrometers will return thousands of spectral observations, and better visualization

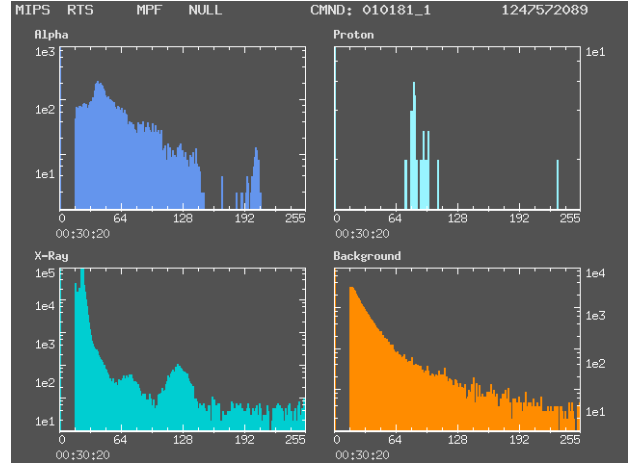


Figure 1. A spectrum chart of APXS data of the rock Yogi from the Pathfinder mission.

modalities are required to support the demanding daily cycle of operations. Mast-mounted spectroscopy of targets far from the rover will need to be quickly analyzed to plan long rover traverses over multiple days during the mission to maximize science return and achieve mission goals.

In this work we will begin with a brief description of rover-based spectrometers. We will then introduce two new spectroscopy visualization techniques that will be used during future rover missions: image cubes and data fusion. Lastly, we summarize the work and briefly mention future directions in data visualization for operations and planning.

2. ROVER-BASED SPECTROMETERS

Like orbital spectrometers, spectroscopy instruments must meet stringent footprint, mass, and power restrictions. Recent advances in this area of technology have produced an impressive array of available instrumentation that meets these requirements and returns superior data yield compared to previous missions. We will now describe several of these instruments in more detail.

The Miniature Thermal Emission Spectrometer (Mini-TES) will be used during the 2003 MER mission [2]. The Mini-TES instrument is a Michelson interferometer with a spectral resolution of 10 cm^{-1} over a range of 5 to $29 \mu\text{m}$. Its field of view is selectable as either 8 mrad or 20 mrad by a field stop in the aperture that is activated by a solenoid. A scanning mirror assembly varies the optical path of the spectrometer, allowing spectra to be sampled along 360° in azimuth and between -50° and $+30^\circ$ in elevation. Since the Mini-TES is a pointing spectrometer located on the Pancam Mast Assembly (PMA), it can be used to identify interesting science targets at

a distance from the rover as well as locations near the rover. Typical Mini-TES usage during the mission will involve sampling grids of thousands of spectra per day.

The MER instrument arm will carry two spectrometers: the Alpha Particle X-Ray Spectrometer (APXS) and the Mössbauer Spectrometer [2]. These spectrometers will make contact with Martian soils and rocks to make mineralogical analyses. The APXS is capable of determining the abundances of almost all rock-forming elements. As its name implies, the APXS can be dynamically configured to emit and sample alpha particles and/or x-rays. The x-ray sensing mode is sensitive to relatively heavy elements like Al, Si, K, Ca, Fe, Na, P, S, Cl, Ti, Cr, and Mn. The alpha mode is sensitive to lighter elements such as C and O. This APXS will have similar capabilities to the one that was used during the Pathfinder mission to sample the composition of atmosphere, soils, and rocks such as Barnacle Bill and Yogi. There have been several improvements to the instrument since the Pathfinder mission [3]. The most noticeable difference is that there is no Proton emission mode in the new APXS. Since Pathfinder, the X-ray sensitivity and spectral resolution of the instrument has been increased to make the proton mode unnecessary. In addition, reference targets on the rover will allow in-situ calibration of the APXS during the mission. Extensive pre-flight calibration will be conducted to reduce sensitivity to electromagnetic interference and Mars ambient conditions. The other arm-mounted spectrometer, the Mössbauer, is well-suited to identify ferrous minerals that are difficult to detect with the APXS. It emits gamma rays from its vibrating ^{57}Co radiation source and classifies minerals based on the vibration velocity of the source when counting the rays that are scattered back to the instrument.

Some of the results in this work are based on data from the Infrared Point Spectrometer (IPS) during the MER-FIDO 2001 field test (FIDO is a prototype Athena-class rover developed at the Jet Propulsion Laboratory). The mast-mounted IPS is sensitive to aqueously-deposited materials such as clays and carbonates as well as igneous minerals. It samples the infrared spectrum from 1.3 to 2.5 microns at 8 nm resolution and reveals mineral content by sensing the reflection and absorption of the infrared energy [4].

3. IMAGE CUBES

Image cubes offer a superior visualization modality to viewing individual spectrum plots. An image cube is a hyperspectral image that is constructed from a collection of spectra that are sampled in a regular grid in azimuth and elevation. Figure 2 shows the layout of an image cube of data from the Mini-TES spectrometer. The horizontal dimension is azimuth, the vertical dimension is elevation, and the depth dimension is wavelength. An image of a particular wavelength of radiance (in azimuth and elevation) is formed by intersecting a plane with the cube that is normal to the wavelength axis. Images in wavelength-elevation or wavelength-azimuth can also be produced by taking a normal plane of the cube to the azimuth or elevation planes, respectively. The dotted lines delineate the edges of the cube and the solid line normal to the plane is

the interactive cursor.

By examining images in the cube at wavelengths of interest, it is possible to identify one interesting spectrum out of thousands in a few seconds. The image plane in the cube is rendered in a 3D user interface and can be quickly scrolled through the available wavelengths. When an interesting image is found, the analyst selects any pixel in the area of interest to produce a spectrum plot at that azimuth and elevation.

Standard image enhancement algorithms like sharpening or contrast stretching can be used to make a given image easier to interpret. False color images are produced from images at different wavelengths to allow color coding of information for faster data analysis.

4. DATA FUSION

A new and very powerful technique for visualizing spectroscopy data is overlaying images of spectroscopy data onto conventional images from a navigational camera, or data fusion. The 3D positions of each pixel in a hyperspectral image from an image cube are computed and projected back through the camera model of a navigational camera image to create an overlay of color-coded spectrum data on a conventional image.

One of the advantages of this mode of visualization is in saving time. During mission science planning, a large part of spectroscopy analysis involves verification of the location of the target that was sampled. During the 2001 MER-FIDO field test, the IPS pointing spectrometer was used to collect spectroscopy data on targets of interest far from the rover to plan traverses. The problem of verifying the locations of the IPS targets was difficult because navigational camera images that were boresighted with the spectrometer were not available in time to plan new rover activities. As a result, the most current spectroscopy data could not be used to plan the next rover operation cycle during the test. Data fusion will allow existing images to be used to validate the pointing of spectroscopy targets by visualizing the co-registration of these data.

Algorithm

Data fusion is a visualization of co-registered images. For any two images, there must be a mapping from a pixel location in one image onto a pixel in the second image. We assume that for any image to be fused onto a second image there is a range map or other similar 3D position information available at each pixel of the first image. We also require the availability of a camera model for the camera that captured the second image. Given these inputs, the general algorithm for data fusion is as follows:

1. For image A to be fused onto image B :
 - (a) Define an image C that is the same size as image B and the same number of bands as image A .
 - (b) For every pixel $p_{u,v}$ in A (where u,v indicate image plane coordinates):

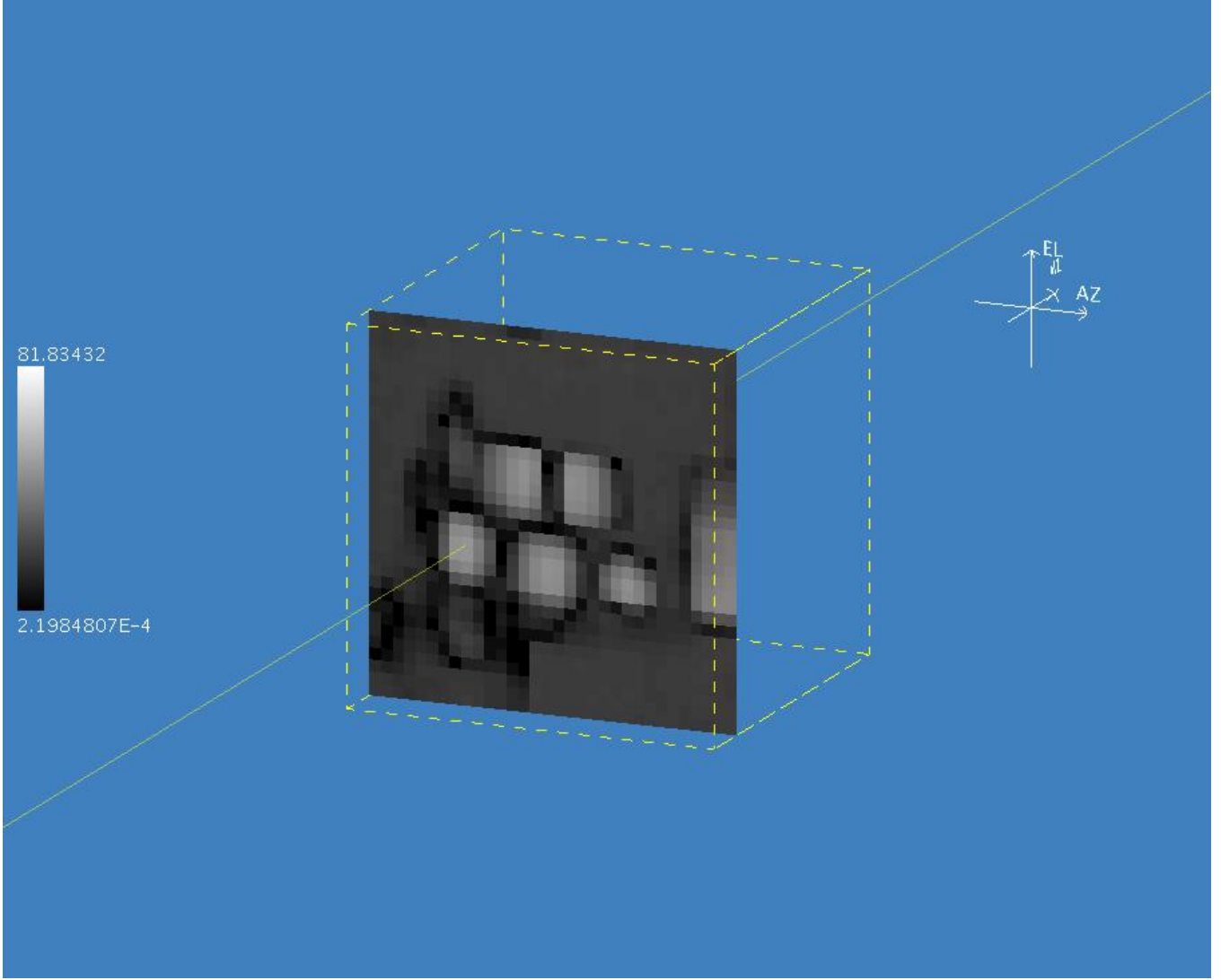


Figure 2. Orthographic view of an image cube of data from the Mini-TES spectrometer. The image plane shown here is in the azimuth-elevation orientation. The dotted lines delineate the cube edges and the solid line normal to the plane is the interactive cursor.

- i. Transform the 3D point $P_{x,y,z}$ corresponding to pixel $p_{u,v}$ to the coordinate frame of the camera that captured B , the transformed point to be denoted $P_{x',y',z'}$.
- ii. Project $P_{x',y',z'}$ through the camera model of image B to the resulting image plane coordinates $p_{u',v'}$.
- iii. If pixel $p_{u',v'}$ lies within the bounds of image B then assign pixel $p_{u',v'}$ in image C the value of $p_{u,v}$ in image A .

If for any pixel in the first image there is no 3D position available (as in the case of a sparse range map), then that pixel will not be overlaid. The larger a region of missing 3D position data, the more noticeable of a hole in the resulting image overlay will be observed. Another implicit assumption at step 1(b)(i) is that the two images to be fused must themselves be co-registered, i.e. the positions and orientations of their cameras relative to each other must be known. We show how this is accomplished using CAHVOR camera models in the next section. If the pixels of the two images have different fields of view this creates a scaling problem for the visualization,

that is when one pixel of the first image maps to many pixels of the second, or vice versa. This can be handled in a number of ways, such as averaging multiple pixels that map to one, or using interpolation to create a smooth image when one pixel maps to many.

Camera Model Back-projection

CAHVOR camera models [5] [6] were designed to make transformations from 3D points to 2D projections (and the reverse) fast and simple. Figure 3 shows a diagram of the CAHVOR camera model. All of the vectors in the model are specified with respect to the world coordinate system (not a camera-centric coordinate system as in many other camera models). \vec{C} is a vector pointing from the origin of an external coordinate system to the first principal point of the camera lens. This represents the position of the camera relative to some meaningful coordinate system in the world, such as the coordinate frame of a rover, or of a site on the terrain. i is

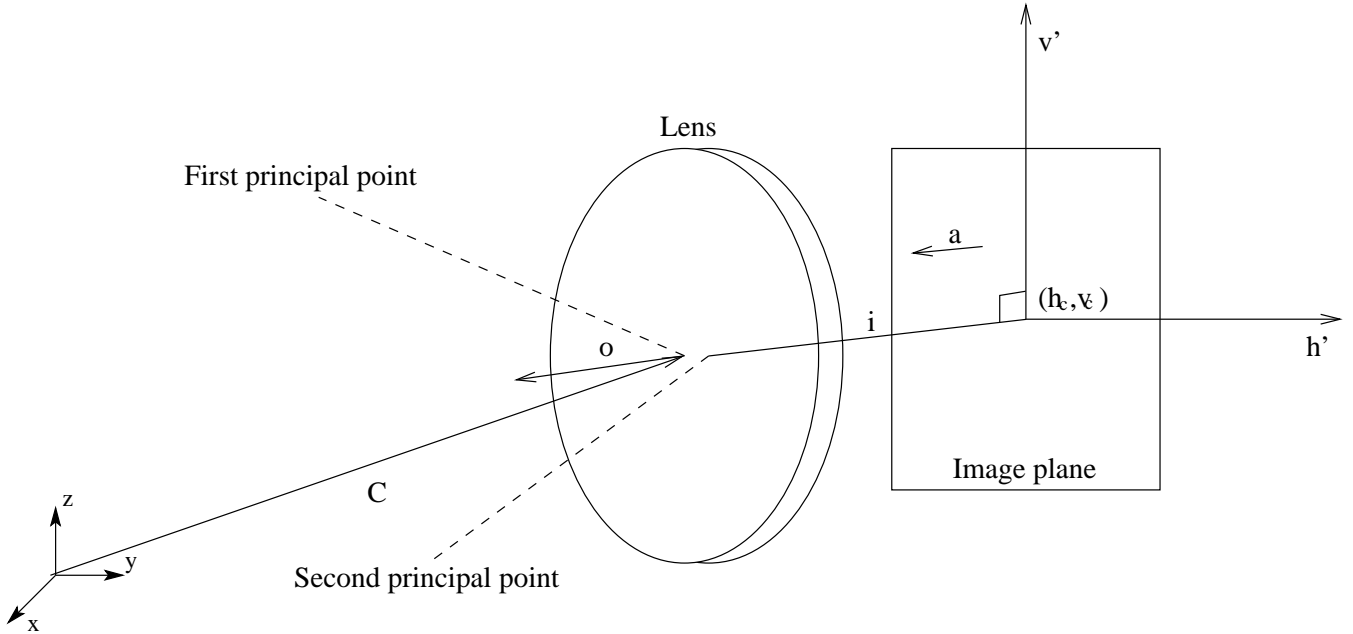


Figure 3. Illustration of the CAHVOR camera model as it relates to the world coordinate frame, optical path, and image plane.

a line segment from the second principal point of the lens to the image plane, perpendicular to it. \vec{a} is a vector parallel to i and pointing into the scene. This represents the pointing orientation of the camera with respect to the external coordinate frame. \vec{h}' and \vec{v}' are vectors that lie parallel to the horizontal and vertical image coordinate system axes and have the same magnitude as i (assuming that the medium is the same on both sides of the lens). These vectors are not necessarily perpendicular. \vec{o} is a vector parallel to the optical axis and pointing into the scene, which is equivalent to \vec{a} if the optical axis is perpendicular to the image plane [6].

Radial lens distortion is also a part of the CAHVOR camera model. This distortion is modeled by a polynomial defined relative to the optical axis \vec{o} (to make it radial). For a particular 3D point p_i , this polynomial is of the form

$$\mu_i = \rho_0 + \rho_1 \tau_i + \rho_2 \tau_i^2 + \dots \quad (1)$$

Where μ_i is a proportionality coefficient, the ρ 's are the radial distortion coefficients, and the τ 's are proportional to the square of λ_i , the perpendicular distance of p_i from the optical axis [5]. The effect of distortion is written as

$$p'_i = p_i + \mu_i \lambda_i \quad (2)$$

Where p'_i is the apparent position of the actual point p_i . To complete the computation of p'_i from the camera model vectors, we use the following additional equations:

$$\omega_i = (p_i - c) \cdot o \quad (3)$$

$$\lambda_i = p_i - c - \omega_i o \quad (4)$$

$$\tau_i = \frac{\lambda_i \cdot \lambda_i}{\omega_i^2} \quad (5)$$

The mapping of a 3D position to its 2D projection (i, j) is then written as

$$i = \frac{(p_i - c) \cdot h}{(p_i - c) \cdot a} \quad (6)$$

$$j = \frac{(p_i - c) \cdot v}{(p_i - c) \cdot a} \quad (7)$$

The vectors \vec{h} and \vec{v} are the horizontal and vertical vectors of the camera model, derived during camera calibration. They are related to \vec{h}' and \vec{v}' in that their projections onto the image plane are equal to \vec{h}' and \vec{v}' , respectively. The complete CAHVOR camera model consists of the five vectors C , a , h , v , o , and the radial distortion coefficients ρ_0 , ρ_1 , and ρ_2 .

5. RESULTS

To demonstrate image cubes and data fusion, we will visualize IPS data with Navcam imagery taken during the 2001 MER-FIDO field test. One particular observation that was made was a 3 by 3 grid of spectra of a rock denoted “sol1-aaron” that resulted from the first day of science planning and operations. The sequence executed on the rover acquired a 3 by 3 grid of spectra centered on the designated target, and

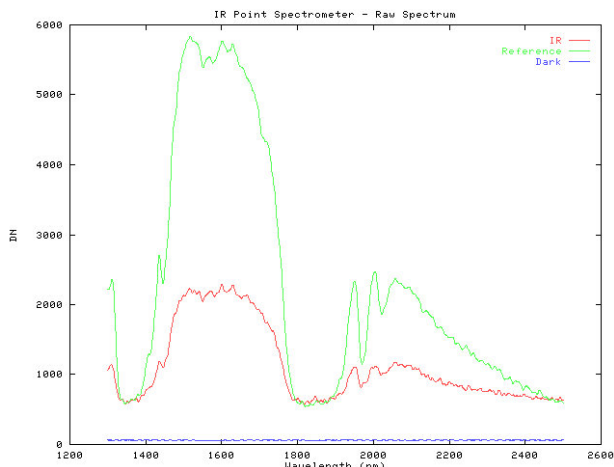


Figure 4. IPS spectrum of target sol1-aaron during the 2001 MER-FIDO field test.

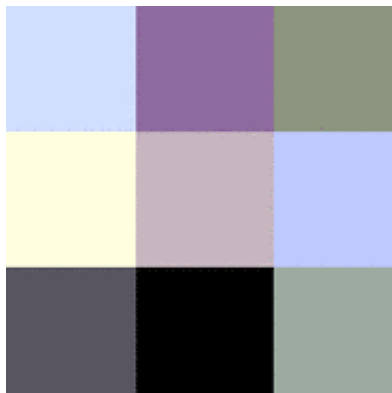


Figure 5. IPS false color image of target sol1-aaron. Red, green, and blue indicate the average radiance over the range 1500-1800, 2000-2200, and 2201-2400, respectively.



Figure 6. Navcam image of target sol1-aaron with 3 by 3 IPS false color spectrum grid overlaid at 100% opacity.

taken with 1 degree horizontal and vertical spacing between observations. An analysis of the spectrum in the center of the grid, shown in Figure 4, shows a ratio of raw radiance to reference radiance of close to 1 in the ranges \sim 1300-1400, \sim 1800-1900, and \sim 2400-2500. We will therefore visualize the data from regions of the spectrum that lie outside these ranges. We chose for our example the ranges 1500-1800, 2000-2200, and 2201-2400, which we assigned to the colors red, green, and blue, respectively. The IPS data was converted into a false color image using an image cube that averaged the radiance values over the three ranges and computed the image, shown in Figure 5.

The false color image itself shows several interesting features. For example, it is evident that the spectrum that corresponds to the bottom-center pixel was in shadow, since there was not enough illumination to produce a substantial radiance value in any of the three wavelength ranges. Further, the various hues in the image are indicative of lesser or greater sensor response in the ranges that are under- or over-represented. For example, the top-center pixel has a purple hue, indicating a stronger response in the first (red) and third (blue) ranges of wavelength that we chose to examine, while the center-left pixel appears yellow, revealing a greater response in the first (red) and second (green) ranges compared to the third. These very different responses may be attributed to the fact the yellow response lays on the rock and the purple response lays on the soil behind it, at least in part. This location information is apparent when we use data fusion to overlay the false color image onto the Navcam image of this target.

Figure 6 shows the overlay of the image in 5 on a (left) Navcam image of target sol1-aaron. Here, we can see that some of the spectra were targeted on the rock, and some lay at least partially on the soil behind the rock. Also, some of the spectra near the bottom were taken in shadow and are less useful for analysis than those in the center row where the illumination was more favorable.

The 3D view shown in 7 shows a different viewpoint of so11-aaron with the IPS data overlaid as a texture map on top of a 3D mesh built using the stereo range data from the Navcam image pair. Here, it is more apparent that the top-left and top-right spectra were taken on the soil behind the rock. Unfortunately, there is incomplete range data to show the entire overlay of the top-center (purple) spectrum, but we can still see that it lays at least in part on the soil behind the rock.

6. SUMMARY

In future Mars planetary rover missions, pointing spectrometers will return volumes of spectroscopy data. This valuable science data can be quickly and effectively visualized as useful information by using advanced visualization techniques such as image cubes and data fusion. Image cubes provide superior visualization over individual spectrum plots by presenting spectra as images that are readily interpreted by humans and can be enhanced using standard image processing algorithms. Data fusion allows mission planners to quickly verify the pointing of spectra using any co-registered navi-

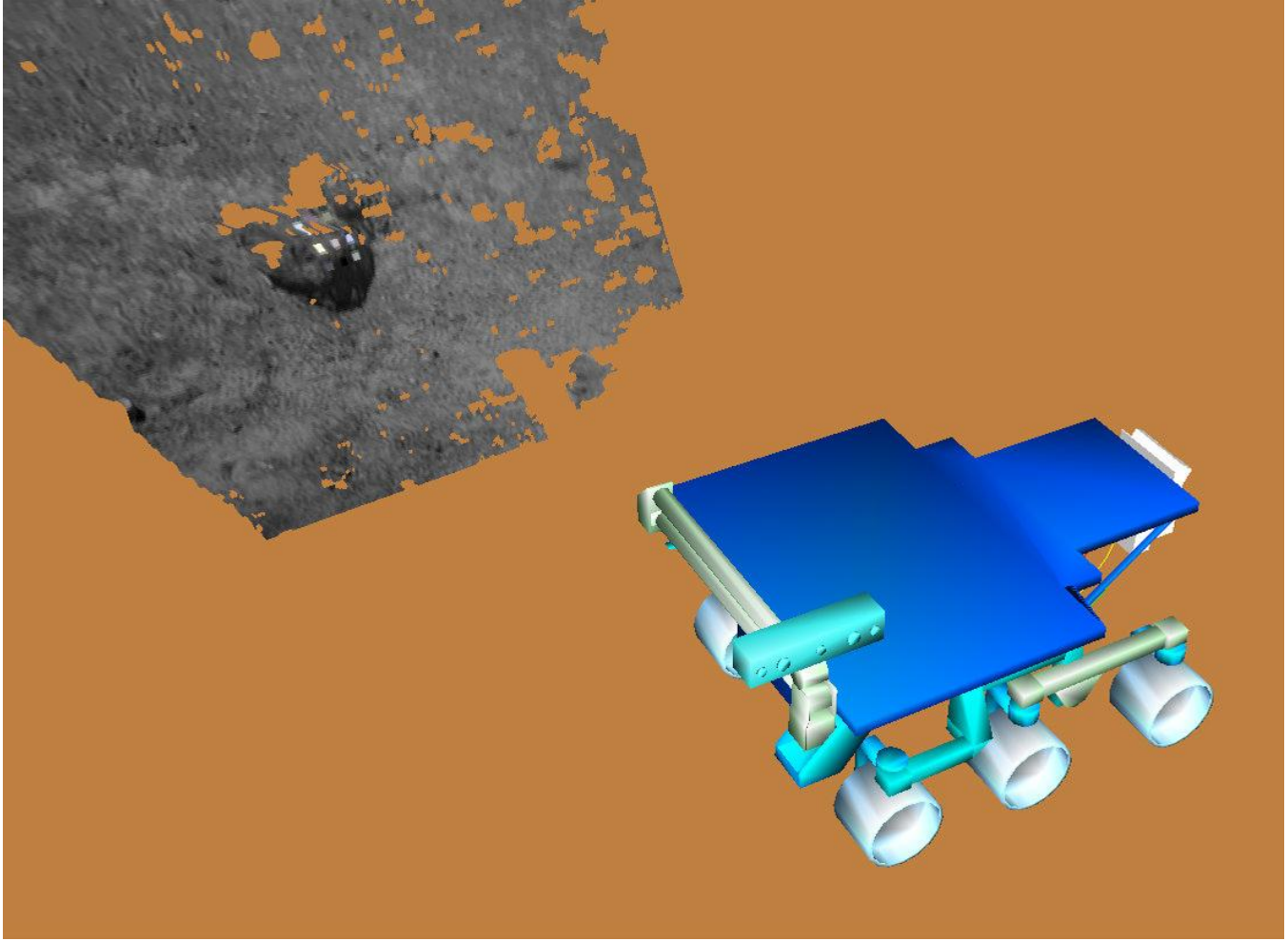


Figure 7. 3D view of the FIDO rover and the Navcam data for target soll-aaron.

gational imagery that is currently available. This will allow the most current spectroscopy data to directly influence rover activity planning on every day of mission operations.

The visualization work documented herein will be implemented as part of the Science Activity Planning (SAP) software to be used during the 2003 Mars Exploration Rover mission. Some future directions of this work will include the fusion of images from multiple cameras on board the rover, as well as with orbital imagery of the rover's current site.

ACKNOWLEDGEMENTS

The research described in this paper was carried out at the Jet Propulsion Laboratory, California Institute of Technology, under a contract with the National Aeronautics and Space Administration. The authors would like to thank Albert Haldemann and Albert Yen of JPL for their contributions of background material on APXS and IPS spectroscopy and Noel Gorelick of Arizona State University for providing a Mini-TES spectral dataset.

REFERENCES

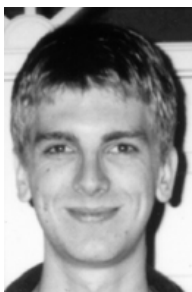
- [1] http://www-pdsimage.jpl.nasa.gov/PDS/internal/MPF/mprv_0001/browser/apxs.htm.
- [2] http://athena.cornell.edu/the_mission/instruments.html.
- [3] http://athena.cornell.edu/the_mission/ins_apxs.html.
- [4] <http://fidoinstruments.jpl.nasa.gov/ips.html>.
- [5] Y. Yakimovsky and R. Cunningham. A system for extracting three-dimensional measurements from a stereo pair of tv cameras. *Computer Graphics and Image Processing*, 7:195–210, 1978.
- [6] D. B. Gennery. Camera calibration including lens distortion. Technical Report JPL D-8580, Jet Propulsion Laboratory, California Institute of Technology, Pasadena, California, May 1991.



Mark Powell is a member of the technical staff in the Autonomy and Control Section at the Jet Propulsion Laboratory, Pasadena, CA since 2001. He received his B.S.C.S. in 1992, M.S.C.S in 1997, and Ph.D. in Computer Science and Engineering in 2000 from the University of South Florida, Tampa. His dissertation work was in the area of advanced illumination modeling, color and range image processing applied to robotics and medical imaging. At JPL his area of focus is science data visualization and science planning for telerobotics. He is currently serving as a software and systems engineer, contributing to the development of science planning software for the 2003 Mars Exploration Rovers and the JPL Mars Technology Program Field Integrated Design and Operations (FIDO) rover task. Dr. Powell received the 2001 Outstanding Dissertation Award from the University of South Florida. He, his wife Nina, and daughters Gwendolyn and Jacquelyn live in Tujunga, CA.



Paul G. Backes is a technical group leader in the Autonomy and Control Section at Jet Propulsion Laboratory, Pasadena, CA, where he has been since 1987. He received the BSME degree from U.C. Berkeley in 1982, and MSME in 1984 and Ph.D. in 1987 in Mechanical Engineering from Purdue University. He is currently responsible for distributed operations research for Mars lander and rover missions at JPL. Dr. Backes received the 1993 NASA Exceptional Engineering Achievement Medal for his contributions to space telerobotics (one of thirteen throughout NASA), 1993 Space Station Award of Merit, Best Paper Award at the 1994 World Automation Congress, 1995 JPL Technology and Applications Program Exceptional Service Award, 1998 JPL Award for Excellence and 1998 Sole Runner-up NASA Software of the Year Award. He has served as an Associate Editor of the IEEE Robotics and Automation Society Magazine.



Jeffrey S. Norris is a computer scientist and member of the technical staff of the Autonomy and Control Section at Jet Propulsion Laboratory. He specializes in software engineering for telerobotics, distributed operations, machine vision, and large scale interfaces. He received his Bachelor's and Master's degrees in Electrical Engineering and Computer Science from MIT. While an undergraduate, he worked at the MIT Media Laboratory on data visualization and media transport protocols. He completed his Master's thesis on face detection and recognition at the MIT Artificial Intelligence Laboratory. He now lives with his wife in Azusa, California.